Oxygen- and photoresist-related interface states of 4H-SiC Schottky diode observed by deep-level transient spectroscopy

Hong Jeon Kang,[1] Jeong Hyun Moon,[2] Wook Bahng,[2] Suhyeong Lee,[1] Hyunwoo Kim,[1] Sang-Mo Koo,[3] Dohyun Lee,[4] Dongwha Lee,[5] Hoon-Young Cho,[5] Jaeyeong Heo,[6,a)] and Hyeong Joon Kim[1,a)]

[1]*Department of Materials Science and Engineering, College of Engineering, Seoul National University, Seoul 08826, South Korea*
[2]*Power Semiconductor Research Center, Korea Electrotechnology Research Institute (KERI), Changwon 51543, South Korea*
[3]*Department of Electronic Materials Engineering, Kwangwoon University, Seoul 01897, South Korea*
[4]*Samsung Electronics, 1, Samsungjeonja-ro, Hwaseong-si, Gyeonggi-do 445-701, South Korea*
[5]*Department of Physics, Dongguk University, Seoul 100-715, South Korea*
[6]*Department of Materials Science and Engineering and Optoelectronics Convergence Research Center, Chonnam National University, Gwangju 61186, South Korea*

(Received 13 June 2017; accepted 21 August 2017; published online 6 September 2017)

Trap levels play an important role in semiconductor power devices. The barrier height of a metal-semiconductor junction, one of the important factors of unipolar devices, is influenced by the trap levels at its interface, i.e., interface states. However, there has not been much research on the interface states of Schottky diodes yet. Here, we report newly found KI_1, KI_2, and KI_3 interface states of 4H-SiC Schottky diodes. We observed their changes after the first deep-level transient spectroscopy measurements, in which temperature rises to 750 K, and discussed the origins of these changes by using X-ray photoelectron spectroscopy and scanning electron microscopy. The KI_1 was related to oxygen and photoresist (PR) residue, the KI_2 was related to oxygen, and the KI_3 was related to the PR residue. *Published by AIP Publishing.* [http://dx.doi.org/10.1063/1.4989912]

I. INTRODUCTION

In power device technology, 4H-SiC has an expanding market share among semiconductor materials owing to its higher temperature, voltage stability and thermal conductivity than that of conventional silicon. It is expected that the compound annual growth rate of the SiC power semiconductor market and the market size in 2021 would be 19% and $550 M, respectively.[1] In semiconductors used for power devices, trap level plays an important role. The conductivity and the optimal working frequency of bipolar devices depend on the recombination time of electron and hole pairs controlled by the concentration of trap levels inside the materials.[2] The barrier height of a metal semiconductor junction, one of the important factors of unipolar devices, is influenced by the concentration of trap levels at its interface, i.e., interface states.[3]

Although deep-level transient spectroscopy (DLTS) can analyze both the bulk trap levels and interface states of a Schottky diode, only a few papers have reported on the interface states of Schottky diodes. In 1987, Zhang *et al.* discussed the possibility of the measurement of interface states using DLTS.[4] The following year, they investigated more about the measurement and showed that the interface states could be revealed by applying a pulse bias as high as the forward bias.[5] After this research, some related works have been conducted.[6,7] In 2002, Castaldini *et al.* reported a basic research on the interface states of the 4H-SiC Schottky diode.[8]

In this study, we report newly found KI_1, KI_2, and KI_3 interface states of 4H-SiC Schottky diodes by DLTS. We also observed the changes in these states after the first DLTS measurements, in which the temperature rises to 750 K, and discussed the origins of these changes by using X-ray photoelectron spectroscopy (XPS) and scanning electron microscopy (SEM).

II. EXPERIMENTAL

The epiwafer was a production grade wafer with a diameter of 100 mm, 4° off-axis, and a 12-μm-thick epilayer, the dopant density of which was $5 \times 10^{15}\,cm^{-3}$. The wafer was diced into 8 mm × 8 mm squares and dipped into acetone in an ultrasonic bath for 10 min, followed by conventional Radio Corporation of America cleaning[9] and immersion in a buffered oxide etchant (BOE) for 1 min. To make an ohmic contact, a 50-nm-thick Ni layer was deposited on a C-face n^+ substrate with an e-gun evaporator at a base pressure of 5×10^{-6} Torr. For metallization, the wafer was annealed by rapid thermal annealing (RTA) at 1000 °C for 2 min in ambient N_2 (60 Torr). The samples were dipped into the BOE again to remove the unwanted oxide produced during the RTA process. For the Schottky contact, a 200-nm-thick Ni was deposited on the Si-face of an epilayer covered by a shadow mask of 1.4-μm-thick photoresist (PR) AZ5214 patterned by positive photolithography. Finally, Schottky contacts with diameters of 1 mm were formed through a lift-off process.

a)Authors to whom correspondence should be addressed: jheo@jnu.ac.kr and thinfilm@snu.ac.kr

TABLE I. Diode name, order of device fabrication, and its purpose.

Diode name	Order of diode fabrication process	Purpose
B_Ni	RTA → BOE → shadow mask → Ni	Control
O_Ni	RTA → shadow mask → Ni → BOE	Impact of unwanted oxide
P_B_Ni	RTA → photolithography → BOE → Ni → lift-off	Impact of PR residue

Three types of diodes were fabricated; the main differences in their processes and purposes are listed in Table I. The B_Ni diodes were fabricated as a control group. The O_Ni diodes were fabricated to observe the effects of oxygen by intentionally leaving the oxide produced during the RTA process owing to the inevitable air leakage through the splices and O-rings of the RTA equipment. The P_B_Ni diodes were fabricated to observe the effect of the PR residue remaining after the photolithography process.

The DLTS was composed of a Boonton 7200 CV meter, an Agilent 81110a pulse generator with an 81111 A channel, a Janis ST-100 cryostat with a Lakeshore 335 temperature controller, a Picoscope 4262 Oscilloscope, and an operating PC. The operating pressure of the cryostat was lower than 1×10^{-3} Torr. To observe the interface states, a quiescent reverse bias of −1.8 V and a filling pulse bias of 1.65 V, as high as the barrier height of Schottky diodes, were applied to fill the interface states with electrons. On the other hand, to observe the bulk trap only, a quiescent reverse bias of −9.3 V and a filling pulse bias of −6 V were applied to prevent electrons from filling the interface states. The pulse width and the period were fixed to 1 ms and 1 s, respectively. In our recent experiments, we have concluded that the interface states could be found by using pulse width shorter than 1 ms.

After the ends of pulse bias, the capacitance values were stored as a function of time and underwent some calculations to obtain the DLTS spectra and enhance the signal-to-noise ratio.[10] The noise was reduced by performing additions and subtractions of the measured capacitance values

$$s(t_i) = \sum_{t=t_i}^{2t_i} C(t) - 0.5 \cdot \sum_{t=2t_i}^{4t_i} C(t), \tag{1}$$

where t is the time elapsed after the end of pulse, t_i is the initial measurement time, and $C(t)$ is the measured capacitance value, which can be related to time t

$$C(t) = C_q + \Delta C(t), \tag{2}$$

$$\Delta C(t) = \Delta C(0) \cdot \exp\left(-\frac{t}{\tau}\right), \tag{3}$$

where τ is the temperature dependent time constant, C_q is the capacitance value at the quiescent reverse bias and ΔC is the differential capacitance which is proportionate to trap density. After combining Eqs. (1)–(3), we get

$$s\{t_i, \tau(T)\} = \Delta C \cdot \left\{ \sum_{t=t_i}^{2t_i} \exp\left(-\frac{t}{\tau}\right) - 0.5 \cdot \sum_{t=2t_i}^{4t_i} \exp\left(-\frac{t}{\tau}\right) \right\}. \tag{4}$$

The bracket on the right term is defined as a weight function w that depends on parameter t_i and τ, which has a mathematical maximum value,

$$\Delta C = \frac{s\{t_i, \tau(T)\}}{w_{max}(t_i)}. \tag{5}$$

ΔC collected from 80 K to 750 K became "one" DLTS spectra. A point of Arrhenius plot could be obtained by matching the theoretical emission rate at w_{max}, determined by t_i, and measured peak-temperature positions of the spectra.[11] The initial time, t_i, was set to 20, 30, 45, 67.5, and 101.25 ms to obtain five points for the Arrhenius plot. The activation energy and capture cross-sections were calculated from the slope and the y-intercept of the Arrhenius plot, respectively, assuming a temperature-independent capture-cross section. The t_i value of the DLTS spectra shown in this research was 45 ms.

The XPS was composed of an ultra-high vacuum analysis chamber, a spherical sector analyzer, and a monochromatic X-ray source. Si 2p, O 1s, and C 1s peaks were analyzed before depositing the nickel Schottky metal to observe the SiC surfaces. SEM (SUPRA 55VP, Carl Zeiss AG) was used to observe the shape of PR patterns after the photolithography.

III. RESULTS AND DISCUSSION

Figures 1(a) and 1(b) show the first and second measurements of the bulk region which is 1.3–1.5 μm below the interface, determined by depletion width calculations. In Figs. 1(a) and 1(b), the known $Z_{1/2}$[12] and $EH_{6/7}$[13] peaks as well as an unknown peak A are found. The peak A could be

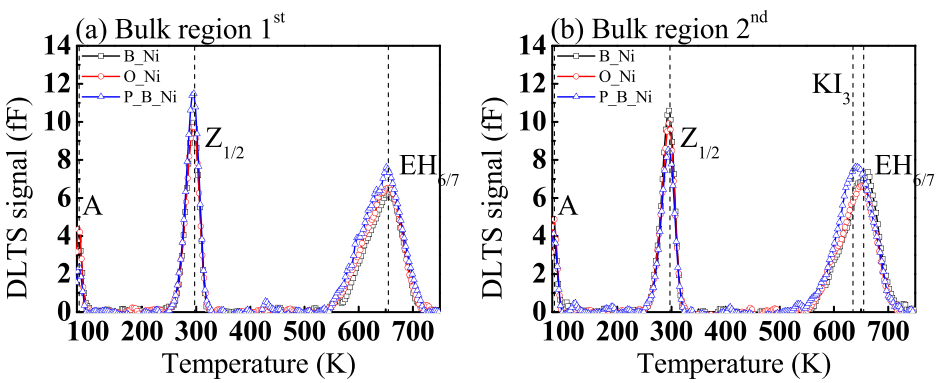

FIG. 1. DLTS spectra of the bulk region for the (a) first and (b) second measurements. The unknown peak A and known $Z_{1/2}$ and $EH_{6/7}$ peaks are found from both measurements. The KI_3 peak arises at the second measurement.

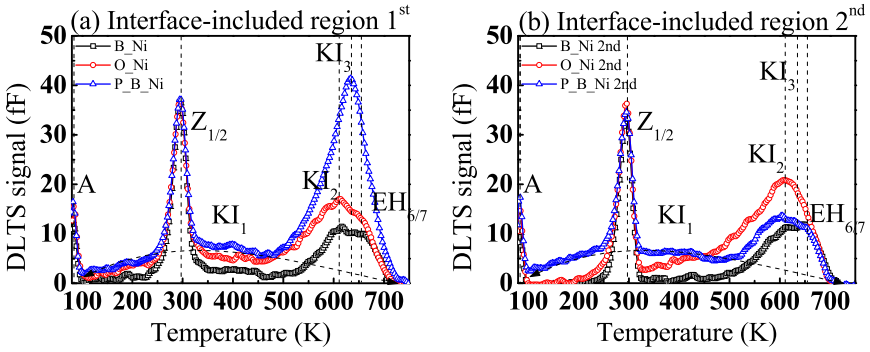

FIG. 2. DLTS spectra of interface-included regions of (a) first and (b) second measurements of the diodes. At the second measurements, KI_1 in B_Ni and O_Ni, and KI_3 peaks in P_B_Ni reduce, while KI_1 in the P_B_Ni shifted toward lower temperatures, and the KI_2 peaks in O_Ni increased.

intrinsic bulk traps in the epilayer, which may be produced during the growth process. Since the KI_3 peak is observed only in the second measurement of the P_B_Ni diode in Fig. 1(b), the KI_3 could be related to a PR residue, which could react with SiC at the interface after the first measurement.

Figures 2(a) and 2(b) show the first and second measurements of the interface-included region, which ranges 0 to 0.8 μm below the interface. In both measurements, the intrinsic bulk traps of A, $Z_{1/2}$, and $EH_{6/7}$ are observed. Additionally, an unknown KI_1 baseline and KI_2 and KI_3 peaks are found.

In the first measurement, the KI_1 baseline of the O_Ni diode is about twice that of the B_Ni diode owing to oxygen. The intensity of the KI_1 baseline of the P_B_Ni diode is the largest owing to the PR residue. The intensity of the KI_2 peak of the O_Ni diode is 1.5 times larger than that of the B_Ni diode owing to the higher oxygen content at the interface. The intensity of the KI_3 peak of the P_B_Ni diode is four times larger than that of the B_Ni diode. Such a large intensity likely originates from the PR residue at the interface.

In the second measurement, the intensity of the KI_1, KI_2, and KI_3 peaks are different from the first measurements. The KI_1 peak of the B_Ni diode vanishes and the same peak of the O_Ni diode is reduced by up to 45%. This may be due to the diffusion of oxygen from the interface into the bulk region after the first measurements. The intensity of the KI_1 baseline on the left of the $Z_{1/2}$ peak of the P_B_Ni diode increases, while the intensity of the KI_1 baseline on the right of $Z_{1/2}$ decreases. Since the PR residue after the first measurement could change its contents by eliminating light compounds,[14] the decrease of the KI_3 peak is likely related to the eliminated organic compounds, while the increase of the KI_1 baseline could be related to the remaining compounds. The KI_2 peak of the B_Ni diode remains the same, and the KI_2 peak in the P_B_Ni diode is observed for the first time after the KI_3 peak vanishes, and its intensity becomes similar to that of the B_Ni diode, which could be due to the similar oxygen content at their interfaces. On the other hand, the KI_2 peak of the O_Ni diode increases by 15% after the first measurement, which may be due to the highest oxygen concentration and its reaction with SiC.

Figures 3(a) and 3(b) show the three different depth regions of the first measurement of the O_Ni and P_B_Ni diodes, respectively. Since the observed depth regions were controlled by the applied reverse bias, which also changes the depletion capacitance and the DLTS signal, the spectra were normalized by each $Z_{1/2}$ intensity to observe relative changes in the intensity of the peaks. These normalized spectra clearly show that the KI_1, KI_2, and KI_3 peaks are present only at the shallow region near the interface. In addition, the reduction of $EH_{6/7}$ near the interface is also noted in the O_Ni diode. The $EH_{6/7}$ has been regarded as an energy level related to carbon vacancies, and it is known to be proportional to the $Z_{1/2}$. Alfieri and Kimoto discussed that the EH_6, which is resolved from the $EH_{6/7}$, may be related to a complex involving the carbon vacancy, since the EH_6 has slightly different behaviors from the $Z_{1/2}$ and the EH_7.[15] Therefore, the relative reduction of the $EH_{6/7}$ observed here suggests the reduction of EH_6. This reduction may be due to different properties between the bulk and the interface, or interaction with the oxygen.

The elevated temperature may have influenced on the location and the intensity of KI_1 and KI_3 peaks during the first DLTS measurement itself. However, the location of the KI_2 peak was consistent for the first and second measurements, which indicates the relative accuracy and stability of KI_2 states.

The Arrhenius plots are shown in Fig. 4: (a) bulk region and (b) interface-included region (0 to 0.8 μm below

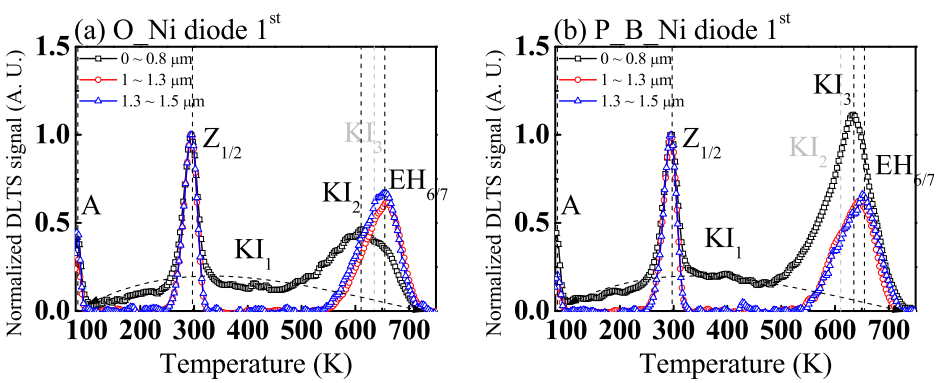

FIG. 3. Normalized DLTS spectra of (a) first and (b) second measurements with three different depth regions, 0 to 0.8 μm, 1 to 1.3 μm, and 1.3 to 1.5 μm, calculated by its depletion width.

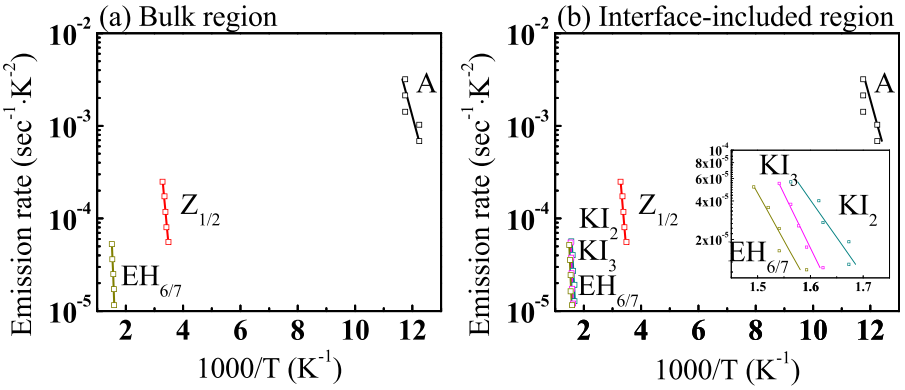

FIG. 4. Arrhenius plots extracted from the DLTS spectra classified into the (a) bulk region and (b) interface-included region (0 to 0.8 μm below the interface). The inset in (b) is the enlargement of the KI_2, KI_3, and $EH_{6/7}$ plots. The open dots are measured values, while the lines are fitted by the least squares method for log fitting.

the interface). The corresponding energy levels and capture cross-sections, calculated from Arrhenius plots, are listed in Table II. Some energy levels and their deviations are unavailable because of the closeness of the peak positions and noise interferences. In that case, a relative peak positions (RPP) at the X-axis in DLTS spectra were introduced; RPP is 0 at the position of the $Z_{1/2}$ peak and 1 at the position of the $EH_{6/7}$ peak. For example, if a peak is present halfway between the $Z_{1/2}$ and $EH_{6/7}$ peaks, then the RPP is 0.5.

The energy levels of the $Z_{1/2}$ and $EH_{6/7}$ peaks are 0.7 and 1.6 eV below the conduction band minimum (E_c), similar to other reports.[12,15] The energy level of the peak A is 0.2 eV below E_c, but the exact origin of this peak is unknown. The KI_1 baselines have broad intensity over the whole temperature range so that they can be regarded as interface states spreading out over the band gap, like interface states of a metal-oxide-semiconductor. The energy level of the KI_2 peak is 1.2 eV below E_c, but there is no report with a similar energy level. The RPP of the KI_2 peak and that of the IN10 peak caused by Al, N, and Ne ion implantations[18] are 98% identical. Therefore, the KI_2 and IN10 peaks may have similar defect structures. Even though the KI_1 and KI_2 peaks were strongly related to oxygen in our research, the oxygen-related energy levels induced by oxidation[16] and oxygen implantation[17] were different from the KI_1 and KI_2 levels. This could be due to the different defect structures at the interface and in the bulk. The energy levels and RPP of the KI_3 peak have no similarity to those in other research. The positions of all the available energy levels in this study and some related energy levels reported by others are summarized as a band diagram of Fig. 5.

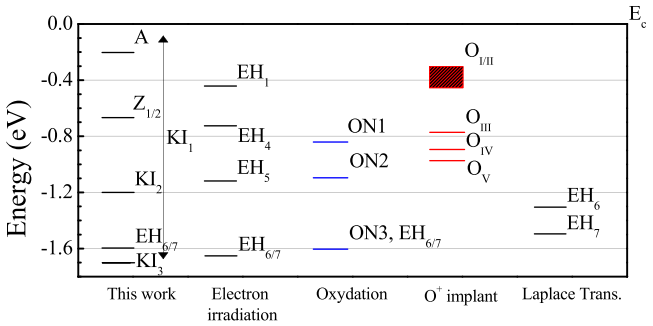

FIG. 5. The trap levels observed in this work and comparable trap levels in other research found by electron irradiation,[13] oxidation,[16] oxygen ion implantation,[17] and Laplace transform.[15]

In order to identify the compositions of the interface of the diodes, the SiC surfaces were analyzed by using XPS just prior to the deposition of nickel. The presence of oxygen on the O_Ni sample is clearly indicated by the strongest Si-O bond in Si 2*p* and O 1*s* peaks of Figs. 6(a) and 6(b), respectively. The intensity of the Si-O bond of the O 1*s* peaks of the B_Ni and P_B_Ni samples could be originated from a native oxide that could be regenerated even after the BOE process. In C 1*s* peaks of Fig. 6(c), the C-C bonds of the B_Ni and P_B_Ni samples are similar to each other, which could be derived from excess carbon. Unlike the C-C bonds of those samples, the Si-C_xO_y bond of the O_Ni sample could be derived from the oxidation of SiC.[19] The presence of PR residue on the P_B_Ni sample cannot be found by the XPS, even though the DLTS spectra of the P_B_Ni diode showed the greatest difference. Therefore, SEM was used to find the trace of any PR residue.

TABLE II. Energy levels, capture cross-sections, and relative peak positions (RPPs) of traps. The deviations of capture cross-sections are in the order of magnitude.

Bulk region			Interface included region			
Trap	Energy (eV)	Capture cross-section (cm^2)	Trap	Energy (eV)	Capture cross-section (cm^2)	Relative peak position
A	0.2 ± 0.04	10^{-11}	A	0.22 ± 0.05	10^{-11}	−0.60
$Z_{1/2}$	0.68 ± 0.04	10^{-14}	$Z_{1/2}$	0.68 ± 0.05	10^{-14}	0.00
KI_1	N/A	N/A	KI_1	N/A	N/A	Continuous
KI_2	N/A	N/A	KI_2	1.2 ± N/A	10^{-17}	0.91
KI_3	N/A	N/A	KI_3	1.7 ± N/A	10^{-13}	0.96
$EH_{6/7}$	1.6 ± 0.1	10^{-13}	$EH_{6/7}$	1.5 ± N/A	10^{-15}	1.00

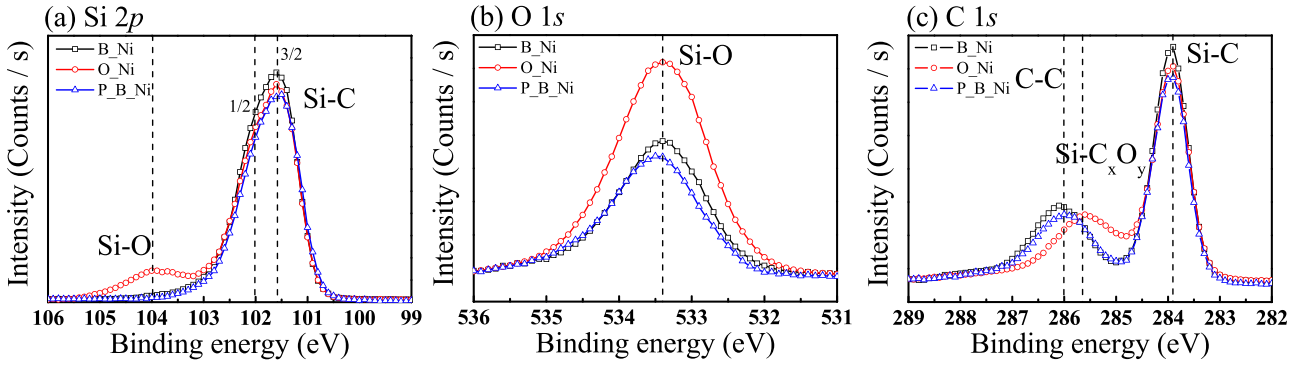

FIG. 6. XPS spectra of (a) Si 2*p*, (b) O 1*s*, and (c) C 1*s* peaks of each sample measured before the Ni deposition.

Figure 7 shows the SEM image of a cross-sectional view of the P_B_Ni sample just after the photolithography process. The yellow circle emphasizes an unintentional edge of the PR pattern that remained even after the nickel deposition and the lift-off process. The edge could influence on the KI_1 and KI_3 peaks of the DLTS spectra.

Figure 8(a) depicts the microstructure of the O_Ni diode before the measurement, in which the amorphous oxide produces the KI_1 states and SiC_xO_y produces the KI_2 states. After the first measurement, the oxygen diffused out and carbon diffused into the interface, as depicted in Fig. 8(b), making the KI_2 peak stronger, while the KI_1 baseline became weaker simultaneously. However, the transformation did not occur completely, since the energy acquisition of the system at 750 K was not sufficient to form the Si-C bond of SiC_xO_y.

Figure 8(c) depicts the microstructure of the P_B_Ni diode before the first measurement, in which the PR residue at the interface could remain and release electrons during the periodic pulse, acting as effective sites for the KI_1 and KI_3 states. After the first measurement, in Fig. 8(d), the elimination of light compounds in the PR residue occurred and reduced the effective sites of KI_1 of baseline on the right of $Z_{1/2}$ and KI_3, while increasing the KI_1 baseline on the left of the $Z_{1/2}$ peak. At the same time, the oxygen in the native oxide diffused from the interface into the bulk region, which could also contribute to the reduction of the KI_1 baseline on the right side of the $Z_{1/2}$ peak.

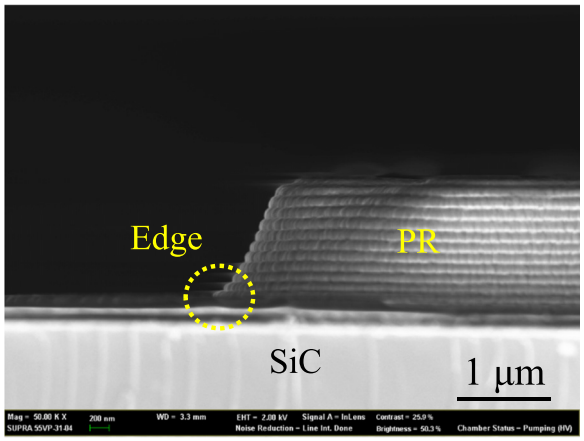

FIG. 7. Cross-sectional SEM image of a patterned PR after photolithography and the developing processes.

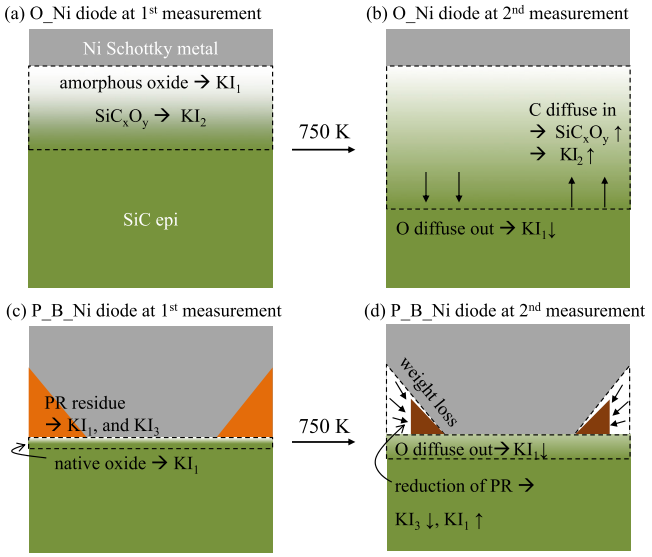

FIG. 8. Schematic explanation for the origins of KI_1 and KI_2 in (a) the O_Ni diode and origins of KI_1 and KI_3 in (c) the P_B_Ni diode at the first measurement. Changes of the origins after the first measurements are illustrated in (b) and (d), respectively.

IV. CONCLUSION

We reported new KI_1, KI_2, and KI_3 interface states of 4 H-SiC Schottky diodes that experienced different processes and discussed their origins while observing the annealing effects at a measurement temperature of up to 750 K. In the first measurements, the oxide at the interfaces produced the KI_1 baseline and the KI_2 peak, and the PR residue at the interface produced the KI_1 baseline and the KI_3 peak. After the first measurements, the amorphous oxide at the interface could partially change to SiC_xO_y, so that the KI_1 baseline decreased, while the KI_2 peak increased. The elimination of light compounds in the PR residue reduced the KI_1 baseline on the right side of $Z_{1/2}$ and the KI_3 peak, while increasing the KI_1 baseline on the left side of $Z_{1/2}$. The KI_1 state was revealed to spread out over the band gap energy. The KI_2 and KI_3 states were located 1.2 and 1.7 eV below the conduction band minimum.

ACKNOWLEDGMENTS

We thank Dr. L. Cohausz in Phys Tech and Mr. Young-Keun Lee in Ginnovation for their critical advice when setting up the DLTS. This work was supported by the World

Premier Materials (WPM) and Tactical core materials technology development projects initiated by the Ministry of Trade, Industry and Energy, Korea and Inter-University Semiconductor Research Center (ISRC) in Seoul National University. J. Heo acknowledges the support by NanoMaterial Technology Development Program through the National Research Foundation of Korea (NRF) funded by the Ministry of Science, ICT and Future Planning (2009-0082580).

[1]See https://www.i-micronews.com/compound-semi-report/product/power-sic-2016-materials-devices-modules-and-applications.html#description for "POWER SiC 2016: Materials, Devices, Modules, And Applications" (last accessed June 6, 2017).
[2]B. J. Baliga, *Fundamentals of Power Semiconductor Devices* (Springer Science & Business Media, 2008), pp. 244, 273.
[3]S. M. Sze and K. K. Ng, *Physics of Semiconductor Devices* (John Wiley & Sons, 2006), p. 139.
[4]H. Zhang, Y. Aoyagi, S. Iwai, and S. Namba, Appl. Phys. Lett. **50**(6), 341 (1987).
[5]H. Zhang, Y. Aoyagi, S. Iwai, and S. Namba, Appl. Phys. A **44**(3), 273 (1987).
[6]F. Hasegawa, M. Onomura, C. Mogi, and Y. Nannichi, Solid-State Electron. **31**(2), 223 (1988).
[7]A. Ahaitouf, E. Losson, and A. Bath, Solid-State Electron. **44**(3), 515 (2000).
[8]A. Castaldini, A. Cavallini, L. Polenta, F. Nava, C. Canali, and C. Lanzieri, Appl. Surf. Sci. **187**(3), 248 (2002).
[9]T. Ohmi, J. Electrochem. Soc. **143**(9), 2957 (1996).
[10]C. Crowell and S. Alipanahi, Solid-State Electron. **24**(1), 25 (1981).
[11]D. Lang, J. Appl. Phys. **45**(7), 3023 (1974).
[12]T. Dalibor, G. Pensl, H. Matsunami, T. Kimoto, W. Choyke, A. Schöner, and N. Nordell, Phys. Status Solidi **162**(1), 199 (1997).
[13]C. Hemmingsson, N. T. Son, O. Kordina, J. Bergman, E. Janzén, J. Lindström, S. Savage, and N. Nordell, J. Appl. Phys. **81**(9), 6155 (1997).
[14]J. A. Lee, S. W. Lee, K.-C. Lee, S. I. Park, and S. S. Lee, J. Micromech. Microeng. **18**(3), 035012 (2008).
[15]G. Alfieri and T. Kimoto, Appl. Phys. Lett. **102**(15), 152108 (2013).
[16]K. Kawahara, J. Suda, and T. Kimoto, J. Appl. Phys. **111**(5), 053710 (2012).
[17]T. Dalibor, H. Trageser, G. Pensl, T. Kimoto, H. Matsunami, D. Nizhner, O. Shigiltchoff, and W. J. Choyke, Mater. Sci. Eng., B **61**, 454 (1999).
[18]K. Kawahara, G. Alfieri, and T. Kimoto, J. Appl. Phys. **106**(1), 013719 (2009).
[19]M. Kim, H. Ju, and J. Kim, Phys. Chem. Chem. Phys. **18**(4), 3331 (2016).